

The influence of buoyant convection on the operation of the upward thermal diffusion cloud nucleation chamber

Frank T. Ferguson

Department of Chemistry, Catholic University of America, Washington, DC 20064

Joseph A. Nuth III

Code 691, NASA-Goddard Space Flight Center, Greenbelt, Maryland 20771

(Received 21 April 1999; accepted 10 June 1999)

Recently, the stable operation of the upward thermal diffusion cloud chamber with respect to buoyancy-induced convection has become a concern in obtaining reliable nucleation data. During chamber operation, evidence of strong convective currents are clearly visible due to the curved trajectories of entrained droplets. A potential problem exists when these flows are much smaller in magnitude; there is no visible evidence of convection, yet these minute flows may result in systematic errors in the nucleation data calculated via 1D diffusive models of the transport mechanisms within the chamber. To examine whether such flows are possible and the characteristics of these flows we have developed an extension to recent 2D modeling of the nucleation chamber which includes buoyancy-induced, convective motion. We have examined both wet and dry chamber operation with an example case of 1-propanol in helium at a pressure of 1.18 bar. In addition, for the dry wall case we examined the effect of overheating the chamber wall and varying the chamber diameter. Results indicate that, for the representative cases investigated, very subtle convective flows can exist and that these minute flows can affect the maximum attainable supersaturation along the chamber centerline. Finally, a list of general recommendations are given for minimizing the possibility of such flows within the cloud chamber. © 1999 American Institute of Physics. [S0021-9606(99)51833-3]

I. INTRODUCTION

The upward thermal diffusion cloud chamber (TDCC) was first developed by Katz and Ostermeir and it has been an elegant tool in the quantitative study of the homogeneous nucleation process.¹ In the past few years this system has been improved and expanded to allow studies of other types of nucleation including photo-² and ion-induced nucleation³ and even the nucleation of high temperature, metallic systems.⁴ One of the most important advantages of the upward thermal diffusion cloud chamber (TDCC) is that it is a steady-state device and experimental conditions can be varied to change the nucleation rate. Also, because of its large diameter to height (D/H) ratio, experimental conditions can be analyzed by solving one-dimensional equations for the energy and mass transport occurring within the chamber.

In the early years of its development, the cloud chamber was used to measure the critical supersaturation, S_{cr} , the supersaturation when the nucleation flux was near $1 \text{ cm}^{-3} \text{ s}^{-1}$. There has been favorable agreement between data collected using the TDCC and the more traditional adiabatic expansion cloud chambers and supersonic nozzles for numerous organic substances.⁵ Later in the 1980's when both the nucleation rate as well as the supersaturation were measured, the diffusion cloud chamber data suggested a dependence upon carrier gas pressure that was not seen in expansion chambers/nozzle experiments.⁶ Since the nucleation rate is extremely sensitive to the temperature and supersaturation, the condensation flux is a much more sensitive indicator of

differences among these systems; small percentage differences in supersaturation can result in order-of-magnitude differences in the the condensation flux.

This dependence upon pressure prompted a series of experiments on the nucleation of materials at elevated pressures.⁷⁻¹⁰ These experiments indicated an increasing value of S_{cr} with total pressure or conversely a decrease in flux with increasing pressure. The experimental results were also dependent upon the type of background gas, namely the S_{cr} vs total pressure variation was greater with helium than with hydrogen.⁸

This pressure dependence as well as the report of a dependence of the nucleation flux upon the degree of heating of the chamber walls prompted Bertelsmann and Heist to develop a more detailed model of the energy and mass transport processes within the TDCC. The authors developed a two-dimensional analog of the 1D model, thereby incorporating the influence of the walls into their analysis.¹¹

Bertelsmann and Heist examined the effect of wet and dry operation (including overheating of the chamber walls), the D/H ratio, and the effect of background gases with 1-propanol. The authors found that the effect of the walls can influence the centerline results if the D/H ratio is not large enough. Therefore it is important to consider this ratio in the design of a chamber and they found that this ratio should be greater than 5 for S_{cr} nucleation measurements and even larger for accurate flux measurements. Whether the TDCC is operated in wet/dry mode did not seem to matter as long as

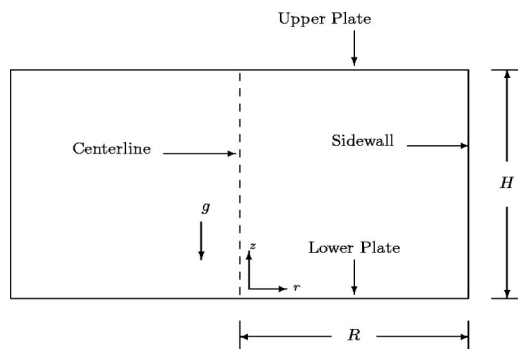


FIG. 1. Cross-sectional diagram of a typical upward thermal diffusion cloud chamber.

the chamber walls are not greatly overheated. In addition, in accordance with experimental observations, their results indicated that the nucleation plane moved towards the upper plate with an increase in the pressure or density of the background gas. Unfortunately, the modeling indicated that even excessive overheating was not able to account for the influence of wall heating upon the nucleation flux which is experimentally observed.

Bertelsmann and Heist noted that the stability of the vapor mixture with respect to buoyant convection is one of the most important issues facing operation of the TDCC. In an accompanying paper, they developed an equation to predict the onset of convection within the chamber.¹²

The work of Bertelsmann and Heist expanded the typical 1D solution to two dimensions, thereby shedding some insight into the influence of the walls on TDCC operation. Unfortunately the model did not include convective effects and these can have a profound effect above and beyond those noted for the diffusive ones. The goal of this work is to extend their work to include buoyant convection and determine its influence upon the temperature and maximum attainable supersaturation within the chamber. Such modeling is important since there is currently some controversy as to whether the nucleation dependence upon pressure is real¹³ (and not included in the classical nucleation development), due to non-ideal gas effects¹⁴ or due to wall/hydrodynamic effects. In this work we will examine several representative cases to determine the kind of flows and influences that are possible. Because of the complexity of the geometry and equations, the goal is not to replace the typical 1D modeling, but perhaps gain some insight on what should be done to keep such simplification valid.

II. MODELING OF THE CLOUD CHAMBER

A. Chamber description

A simplified cross-sectional diagram of a typical TDCC is shown in Fig. 1. The chamber consists of upper and lower plates separated by an annulus. The inside diameter of these plates is denoted by D and the height of the annulus is H . The bottom plate is covered with a thin pool of the liquid to be studied and the chamber volume is filled with a noncondensable, nonreacting carrier gas at a specified pressure. These pressures are typically at or below ambient pressure,

but in recent years Heist has developed a high pressure cloud chamber (HPCC) that can be operated at elevated pressures.⁷

During operation, the temperatures of the two plates are adjusted such that the lower plate is warmer than the upper plate. Vapor leaving the lower pool migrates toward the cooler, upper plate where it condenses and forms a thin film on the upper plate. If the vapor in the chamber is sufficiently supersaturated, isolated droplets can form which fall into the pool of liquid on the lower plate, thus providing a continuous system.

Until recently, the TDCC has only been operated in the dry wall mode. In dry wall operation, the chamber sidewalls are heated just enough to prevent condensation on the walls and this configuration has the advantage that it allows a clearer view of the inside of the chamber. Because of concerns of possible influences on the data due to heating of the walls, Heist *et al.* have recently started collecting data under wet mode operation.⁷⁻¹⁰ In this configuration, chamber sidewalls are not heated and the condensing vapors are allowed to condense and “wet” the chamber sidewalls.

By solving the equations governing the energy and mass transport within the chamber, it is possible to calculate the conditions under which the material condenses. This analysis is simplified by making the chamber diameter to height (D/H) ratio so large that wall effects can safely be ignored and the system can be modeled as a 1D system.

In this work we will examine the same baseline case as studied by Bertelsmann and Heist, namely, 1-propanol in helium at 1.18 bar with lower and upper temperatures of 302.9 and 256.6 K, respectively. This will facilitate direct comparisons with their work. Bertelsmann and Heist’s experimental data for this system were collected using the HPCC and the wet wall configuration. They report that the inside diameter of this chamber is 10.38 cm and, after accounting for the height of the liquid pool, have a $D/H = 7.5$.⁷ These dimensions will be used in this work for the size of the chamber. The nucleation chamber is assumed to be oriented such that the gravitational acceleration is exactly normal to the chamber’s upper and lower plates. Therefore the chamber can be modeled in two dimensions only.

B. Governing equations

It is assumed that the condensation flux is low and hence significant condensation effects can be ignored (i.e., heat of condensation, multiphase flow). The governing equations for this binary system of condensable vapor, a , and background, carrier gas, b , are

continuity equation:

$$\frac{1}{r} \frac{\partial(r\rho u)}{\partial r} + \frac{\partial(\rho v)}{\partial z} = 0, \quad (1)$$

r -momentum:

$$\frac{1}{r} \frac{\partial(\rho r u)}{\partial r} + \frac{\partial(\rho v u)}{\partial z} = -\frac{\partial P}{\partial r} - \left[\frac{1}{r} \frac{\partial(r\tau_{rr})}{\partial r} - \frac{\tau_{\theta\theta}}{r} + \frac{\partial\tau_{rz}}{\partial z} \right], \quad (2)$$

z -momentum:

$$\frac{1}{r} \frac{\partial(\rho r v)}{\partial r} + \frac{\partial(\rho v v)}{\partial z} = -\frac{\partial P}{\partial z} - \left[\frac{1}{r} \frac{\partial(r \tau_{rz})}{\partial r} + \frac{\partial \tau_{zz}}{\partial z} \right] + \rho g_z, \quad (3)$$

energy equation:

$$\frac{1}{r} \frac{\partial(\rho r C_p T)}{\partial r} + \frac{\partial(\rho v C_p T)}{\partial z} = \left[\frac{1}{r} \frac{\partial}{\partial r} \left(k r \frac{\partial T}{\partial r} \right) + \frac{\partial}{\partial z} \left(k \frac{\partial T}{\partial z} \right) \right], \quad (4)$$

conservation of species a :

$$\frac{1}{r} \frac{\partial(\rho r w_a)}{\partial r} + \frac{\partial(\rho v w_a)}{\partial z} = \left[\frac{1}{r} \frac{\partial}{\partial r} \left(D_{ab} r \frac{\partial w_a}{\partial r} \right) + \frac{\partial}{\partial z} \left(D_{ab} \frac{\partial w_a}{\partial z} \right) \right], \quad (5)$$

equation of state:

$$\rho_i = \frac{P_i M w_i}{RT}, \quad (6)$$

and

$$\rho = \rho_a + \rho_b. \quad (7)$$

In these equations r and z are radial and axial coordinates, u and v are the radial and axial velocity components, P the pressure, τ the stress tensor, w_a the mass fraction of component a , and T the temperature. The transport properties used in these equations are ρ , the density, μ , the viscosity, k , the thermal conductivity, C_p , the heat capacity, and D_{ab} the binary diffusion coefficient. It is also assumed that the coupling effects between the mass and temperature fields (soret/dufour effects) are negligible.

In terms of the velocity components the stress tensor components are

$$\tau_{rr} = -\mu \left[2 \cdot \frac{\partial u}{\partial r} - \frac{2}{3} \left(\frac{1}{r} \frac{\partial}{\partial r} (r u) + \frac{\partial v}{\partial z} \right) \right], \quad (8)$$

$$\tau_{\theta\theta} = -\mu \left[2 \cdot \frac{u}{r} - \frac{2}{3} \left(\frac{1}{r} \frac{\partial}{\partial r} (r u) + \frac{\partial v}{\partial z} \right) \right], \quad (9)$$

$$\tau_{zz} = -\mu \left[2 \cdot \frac{\partial v}{\partial z} - \frac{2}{3} \left(\frac{1}{r} \frac{\partial}{\partial r} (r u) + \frac{\partial v}{\partial z} \right) \right], \quad (10)$$

$$\tau_{rz} = \tau_{zr} = -\mu \left[\frac{\partial u}{\partial z} + \frac{\partial v}{\partial r} \right]. \quad (11)$$

Two important simplifications of the above equations should be noted. First, if the gravitational term is set to 0, buoyancy effects are eliminated, Eqs. (1)–(3) drop out and all velocity components are zero (for the boundary conditions in this work). The temperature and mass fraction profiles are still coupled, but only depend upon the diffusive

contributions in Eqs. (4) and (5). Further, if the D/H ratio is extremely large, the equations reduce to the simple one-dimensional form.

C. Boundary conditions

The boundary conditions for the governing equations are very nearly identical to those Bertelsmann and Heist used in their analysis of the cloud chamber; the biggest difference is the need for additional boundary conditions for the momentum components.

1. Upper plate

At the upper plate, the temperature is fixed while the mole fractions of the vapor are given by the ratio of the vapor pressure to the total chamber pressure. In typical TDCC modeling it is customary to use mole fractions and write the mass transport equations in terms of these mole fractions. Because mass averaged velocities are needed for the momentum equations, it is simpler to use mass fractions throughout and the mole fraction boundary conditions are converted to mass fractions. Hence it is useful to define the function, W_x , which indicates a conversion from mole fractions to mass fractions for the binary mixture. Using this newly defined function,

$$T = T_{\text{upper}}, \quad (12)$$

and

$$w_a = W_x \left[\frac{P_{\text{eq}}(T)}{P_{\text{total}}} \right]. \quad (13)$$

Also, it is assumed that there is no slip on the top plate so that $u = v = 0$.

2. Lower plate

The boundary conditions for the lower plate are similar to the upper plate, i.e.,

$$T = T_{\text{lower}} \quad (14)$$

and

$$w_a = W_x \left[\frac{P_{\text{eq}}(T)}{P_{\text{total}}} \right]. \quad (15)$$

Unlike the upper plate, the bottom plate is covered with a liquid pool of the condensible material/species so it is possible to have nonzero velocities at the interface. Since the liquid layer is very thin, it is assumed to first approximation that the velocity components at this interface are zero.

3. Centerline

At the centerline there is neither radial heat nor mass flux; hence

$$\frac{\partial T}{\partial r} = \frac{\partial w_a}{\partial r} = 0. \quad (16)$$

Also, the radial velocity is zero at the centerline while the gradient of the axial velocity is zero

$$u = \frac{\partial v}{\partial r} = 0. \quad (17)$$

4. Sidewall

The nucleation chamber can be operated in either the dry or wet configuration. The boundary conditions for the temperature and mass fraction differ in both cases and are discussed below. In both cases the velocity components at the wall are assumed to be zero.

5. Dry operation

In the dry wall configuration the walls are heated to prevent condensation, hence the supersaturation at every point along the wall must be ≤ 1.0 .

This temperature will be denoted by T_{eq} , the temperature needed to produce a supersaturation of 1.0. Hence,

$$T = T_{\text{eq}} \quad (18)$$

and

$$w_a = W_x \left[\frac{P_{\text{eq}}(T)}{P_{\text{total}}} \right]. \quad (19)$$

6. Sidewall-wet operation

During wet operation of the TDCC, the chamber sidewalls are not heated and the condensing vapors are allowed to wet the chamber sidewalls. It is assumed that the vapor pressure of the condensing vapor is in equilibrium with the liquid at the sidewall temperature, T , or

$$w_a = W_x \left[\frac{P_{\text{eq}}(T)}{P_{\text{total}}} \right]. \quad (20)$$

Unfortunately, the sidewall temperature itself is more difficult to prescribe. The temperature at the chamber sidewall will depend on a variety of factors including condensational heating and convective losses to or gains from the ambient. For now, we adopt the same boundary condition as Bertelsmann and Heist, namely,

$$\frac{\partial T}{\partial r} = 0, \quad (21)$$

but we shall discuss the appropriateness of this boundary condition later in the results section.

D. Physical properties

Physical properties for 1-propanol, including the vapor pressure and binary diffusion coefficient for the helium-propanol system, are taken from the expressions used by Heist *et al.*⁷ Helium physical properties are taken from published fits to experimental data and these fits are listed in Table I.

To calculate the viscosity of the 1-propanol/He mixture, the method of Wilke is used¹⁶

$$\mu_{\text{mix}} = \sum_{i=1}^n \left[\frac{X_i \mu_i}{\sum_{j=1}^n X_j \phi_{ij}} \right], \quad (22)$$

where

TABLE I. Table of helium physical properties used in this work. Data are given for the thermal conductivity, k , (W/m K), viscosity, μ , (cP), and heat capacity, C_p , (J/mole K).^a

Helium-Component b
$k(T) = 1.5703220 \times 10^{-2} + 6.7502003 \times 10^{-4}T$ $- 1.1871593 \times 10^{-6}T^2 + 1.6446470 \times 10^{-9}T^3$ $- 8.0368411 \times 10^{-13}T^4$
$\mu(T) = 3.5938084 \times 10^{-5} + 6.3346898 \times 10^{-7}T$ $- 3.4099052 \times 10^{-10}T^2 + 1.2421068 \times 10^{-14}T^3$
$C_p(T) = 20.786$

^aReference 15.

$$\phi_{ij} = \frac{1}{\sqrt{8}} \left(1 + \frac{M_{w_i}}{M_{w_j}} \right)^{-1/2} \left[1 + \left(\frac{\mu_i}{\mu_j} \right)^{1/2} \left(\frac{M_{w_j}}{M_{w_i}} \right)^{1/4} \right]^2 \quad (23)$$

and n is the number of components. An analogous expression is used for the thermal conductivity of the vapor/gas mixture¹⁶

$$k_{\text{mix}} = \sum_{i=1}^n \left[\frac{X_i k_i}{\sum_{j=1}^n X_j \phi_{ij}} \right]. \quad (24)$$

In this equation the same expression for ϕ is used as for the viscosity, i.e., Eq. (23) and the pure component viscosities are determined from the expressions given in Ref. 7 and Table I.

E. Solution method

The governing equations are solved numerically using finite differences and the semi-implicit method for pressure linked equations (SIMPLER) technique. This technique has been thoroughly discussed in the literature and will not be discussed in detail here.¹⁷ Briefly, the SIMPLER technique employs a staggered grid where pressure and temperature nodes are placed at the center of control volumes and the velocity components are positioned at the faces of these volumes. In this work the resulting discretized equations are solved on a 60×60 grid using a line method and iterations are continued until convergence. Convergence is defined by two criteria: first, the continuity requirement is satisfied (within a specified limit) for every cell in the computational domain, and second, the global energy balance for the system (heat flux in = heat flux out) must agree to within 0.005%.

III. RESULTS

A. Dry wall boundary condition

As stated earlier, during dry wall operation the chamber walls are heated such that the supersaturation at the wall is ≤ 1.0 . The condition where $S = 1.0$ at all points along the sidewall represents an ideal case where the walls are heated just enough to prevent condensation; in actual operation, the wall will almost certainly be hotter than this case.

Figure 2 is a collection of contour plots from a simulation of the dry wall chamber operation for 1-propanol in helium at 1.18 bar. This case is identical to that of the base-

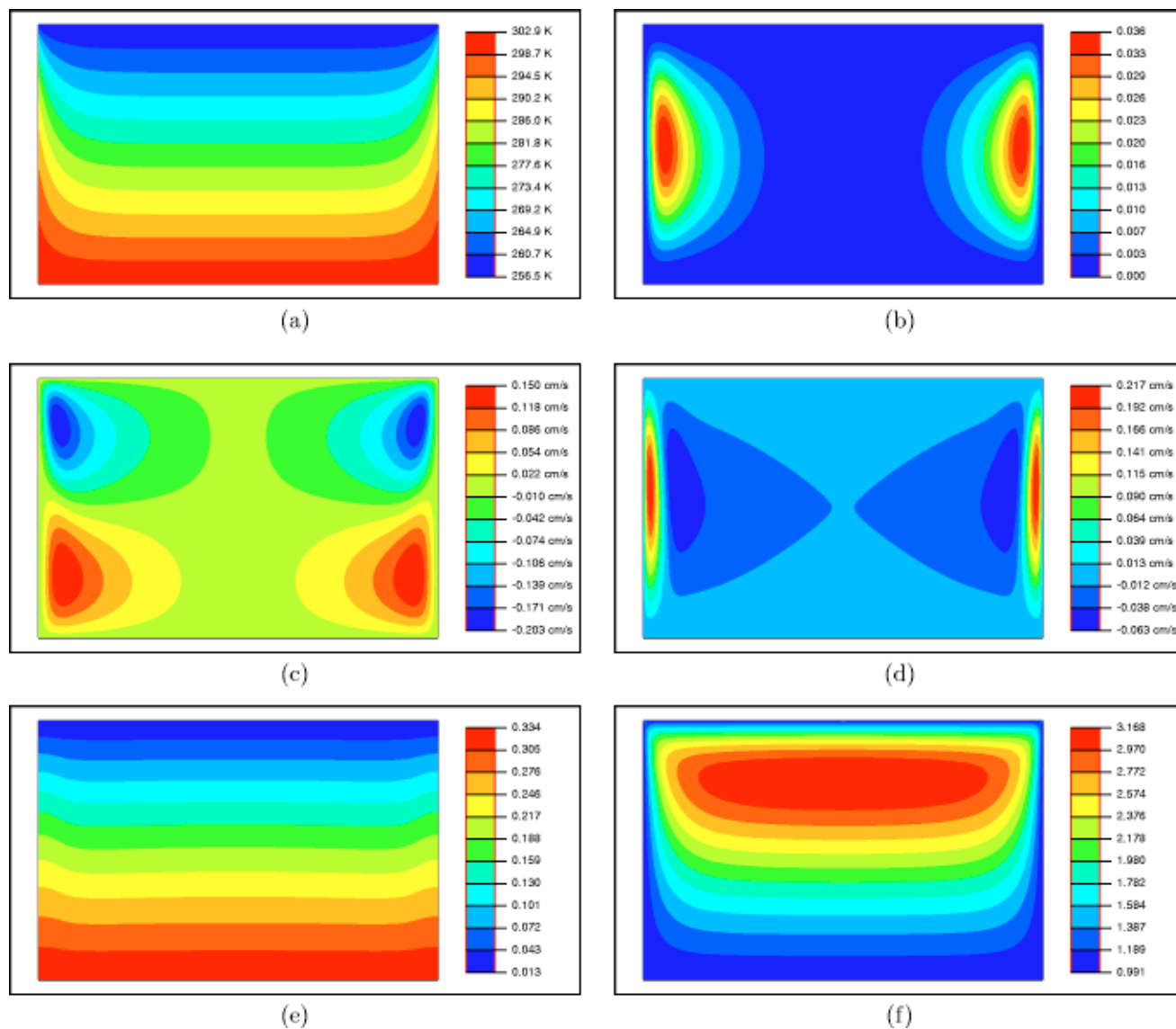


FIG. 2. Contour plots for the critically heated, dry wall operation TDCC for 1-propanol in helium at 1.18 bar. Plots shown above are (a) temperature, (b) streamfunction, (c) r -component of velocity (u), (d) z -component of velocity (v), (e) mass fraction of 1-propanol, and (f) supersaturation.

line case used by Bertelsmann and Heist and will also be used as a baseline case in this work for direct comparison. The contour plots consists of (a) temperature, (b) streamfunction, (c) r -component velocity (u), (d) z -component velocity (v), (e) mass fraction of 1-propanol, and (f) the supersaturation profile.

Throughout most of the chamber the isotherms are flat and layered, but at the sidewall there is a steep gradient in the temperature field. This gradient induces a single convective cell as shown in the streamline plot of Fig. 2(b). There is a steep gradient in the streamlines at the sidewall with a much shallower gradient towards the centerline. These are indicative of a strong upward flow extremely close to the sidewall with a slower, but farther reaching downward flow. These same observations are shown in a different form in the individual momentum components. Figure 2(d) shows the extremely sharp, strong upward flow clinging to the sidewall balanced by a much wider and slower downward flow along the centerline.

The mass fraction profile is layered with no gradient at the wall as dictated by the boundary conditions. The concentration at the sidewall is slightly higher than would be given by diffusion alone. The strong upward flow at the sidewall tends to pull the lines of constant mass fraction away from the lower plate and bunch them slightly at the top plate.

Figure 2(f) shows the result of the convective flow on the predicted supersaturation profile. In the model, convective flows can be conveniently eliminated by setting the gravitational level to zero. Therefore, the changes due to convective effects can clearly be seen by setting the gravitational levels to 0 and 1 and comparing the results. For the 0g case the maximum attainable supersaturation is 3.224. With the convective flows, this maximum is reduced to 3.168—a slight, $\sim 2\%$ reduction.

The radial velocity component, u , is very nearly zero along the centerline. Therefore, flow in this region is dominated by the broad, downward axial velocity component, v . It is possible that visual evidence of such a flow would be

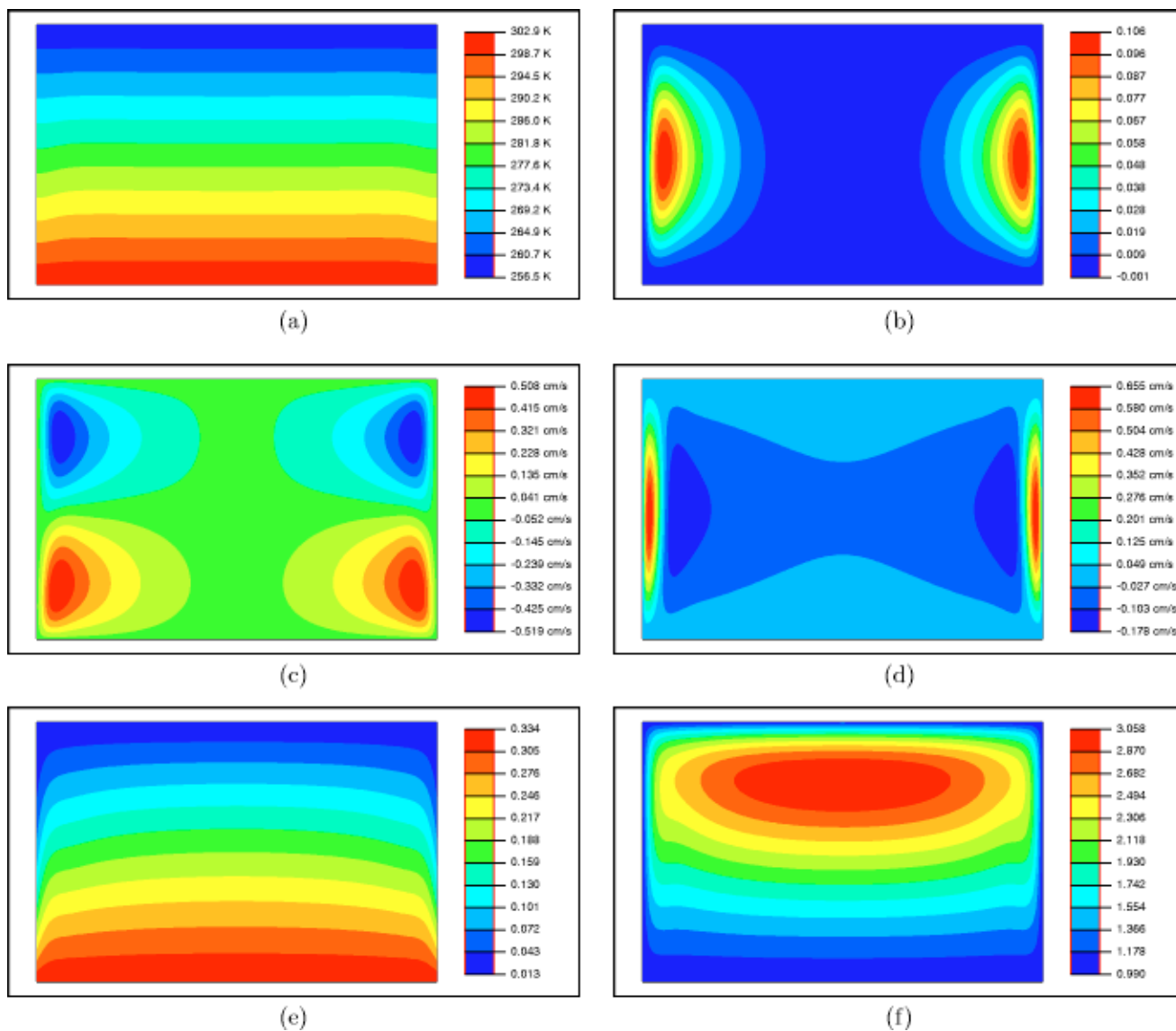


FIG. 3. Contour plots for the wet wall operation TDCC for 1-propanol in helium at 1.18 bar. Plots shown above are (a) temperature, (b) streamfunction, (c) r -component of velocity (u), (d) z -component of velocity (v), (e) mass fraction of 1-propanol, and (f) supersaturation.

difficult to find in an experiment. The flow along the centerline is very weak and nearly “plug-like,” i.e., the radial variation of the v -velocity is very slight. Therefore, the path of any entrained drops along the centerline would tend to be fairly straight and the drops would seem to be falling.

It is not difficult to envision agreement between the flow fields given in Fig. 2 and what is typically observed experimentally with heated side wall operation. During stable dry wall operation, the droplets that form in the center of the chamber fall downward in a straight path to the liquid pool below. There is however a small region close to the chamber walls where there is no nucleation.¹⁸

B. Wet wall boundary condition

Figure 3 is a collection of contour plots for the wet wall case. In this case, there is a minimum disturbance to the temperature field and a maximum disturbance to the concentration profile. In Fig. 3(a), the isotherms are fairly flat with some distortion towards the lower sidewall. If the velocities

were zero, the isotherms would be perfectly flat, and in effect plane-parallel. Because the upward flow increases the transport of propanol along the sidewall, the concentration of propanol is just slightly elevated. In order to satisfy the condition that $S=1.0$ at the wall, the temperatures are slightly elevated along the sidewall.

Buoyant convection is driven by differences in density and convective currents will work to eliminate such density differences. In the dry wall case, differences in density induced by the temperature field caused a slight distortion in the concentration profile along the wall. In a similar fashion, for the wet wall case, differences in density caused by the concentration gradient cause a slight distortion in the temperature field.

The appearance of the flow in this wet wall case is extremely similar to the dry wall case, but the magnitude of the flow is stronger. There is still strong flow very close to the sidewall balanced by a broader, slower flow along the cen-

terline. The downward flow in this case extends a bit farther toward the centerline.

The lines of constant mass fraction of propanol are not as flat as in the dry wall case and the maximum attainable supersaturation is $\sim 5\%$ lower than the value calculated with no convection. Also because the mass fraction profile is not as flat as in the dry wall case, the region of maximum supersaturation for the wet wall case does not extend as close to the walls as in the dry wall case.

For wet wall operation the temperature boundary condition, $\partial T/\partial r=0$, is probably the most debatable boundary condition used in this work. It implies that the chamber walls are perfectly insulating and that no heat is lost to or gained from the ambient environment. Although losses/gains from the sidewalls may be low, it is unlikely that the sidewalls are perfect insulators. The actual temperature profile along the chamber sidewall will depend upon vapor condensation effects, the thickness and conductivity of the sidewall, the ambient temperature, etc. Therefore it is important to consider these possible changes in the temperature field at the side wall when there are large temperature differences between the chamber side walls and the ambient.

C. Effect of wall heating

To examine the effect of chamber sidewall overheating, Bertelsmann and Heist used a complex overheating function which was able to simulate the effects of multiple heating wires and various degrees of overheating. Since their results showed that perturbations due to multiple heating zones tended to be confined to regions extremely close to the chamber sidewall, we decided to use a similar, yet simpler overheating function than Bertelsmann and Heist, namely,

$$T = T_{\text{eq}} + \Delta T_{\text{overheat}} \sin\left(\frac{2\pi z}{H}\right). \quad (25)$$

This function is intended to simulate the effect of a single heating zone. At the top and bottom of the chamber sidewalls there is no disturbance to the sidewall temperature, but the maximum difference between the critically heated walls (T_{eq}) is given by $\Delta T_{\text{overheat}}$ and occurs at the midpoint of the chamber.

Figure 4 is a plot of the reduced supersaturation as a function of degree of overheat for three different chamber D/H ratios. The reduced supersaturation is defined here as the ratio of the maximum attainable supersaturation to the maximum attainable supersaturation calculated via setting the gravitational level to zero. Again, since the same physical properties are used in each case ($g=0,1$), the effects due to convection alone can clearly be seen. It has also been verified that the maximum attainable supersaturation calculated by setting the gravitational level to zero is also equal to the answer obtained by a one-dimensional solution of the equations for the baseline case. The data given in Fig. 4 are based on a chamber diameter of 10.38 cm and D/H ratios of 7.5, 10, and 15. For $D/H=10$ and 15, the reduced supersaturation is very nearly 1.0 even for considerable overheating. There is a slight, noticeable decrease in this reduced supersaturation with heating for the $D/H=10$ case, though. For

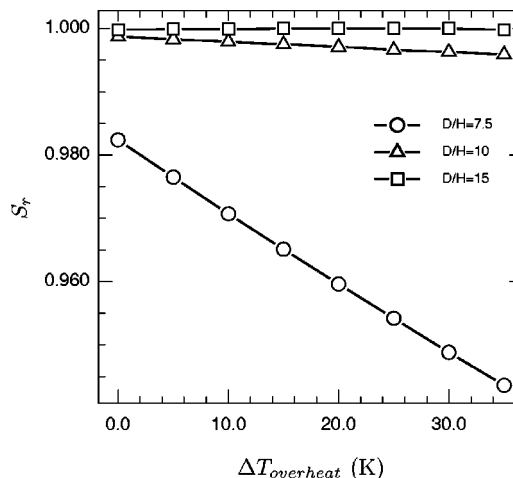


FIG. 4. Effect of chamber overheating on reduced supersaturation ratio. Results are shown for aspect ratios of $D/H=15$, $D/H=10$, and $D/H=7.5$.

the case $D/H=7.5$, there is a more significant reduction in the reduced supersaturation with increasing heating. As shown earlier, there is an approximately 2% reduction in the maximum attainable supersaturation even at the critically heated (i.e., $\Delta T_{\text{overheat}}=0$) case. As the degree of overheating is increased there is a corresponding decrease in the maximum supersaturation. At the highest overheating investigated, $\Delta T_{\text{overheat}}=35$ K, there is nearly a 6% decrease in the maximum supersaturation over what would be calculated by the typical one-dimensional model. Although these are very slight reductions in the supersaturation, the resulting changes in the flux should be much more significant.

These results indicate that buoyant convection is a likely culprit for the experimental observation of a flux dependence on wall heating. In the $D/H=7.5$ case of Fig. 4 a lowering of supersaturation with an increase in wall heating would result in a lower flux. It should be noted that specification that $D/H \geq 10$ is not general and that the results in Fig. 4 are for a specific case (1-propanol in He) under certain conditions; for other substances or chamber configurations, the resulting convective flows may be much smaller or larger.

D. Effect of chamber size

Unlike the one- and two-dimensional conduction solutions used previously, for a given aspect ratio, it is possible for the temperature and supersaturation profiles to depend upon chamber size. A clarification of this statement will be given in a later section. To examine the magnitude of this effect we have maintained the aspect ratio at 7.5 as a baseline case and varied the chamber diameter from 1 to 40 cm. Results are shown in Fig. 5 along with similar results for aspect ratios of 10 and 15.

As shown in Fig. 5, the reduced supersaturations for all aspect ratios converge to 1.0 for very small chamber sizes. As the chamber volume is reduced, viscous drag with the chamber boundaries dominates and the flow field solutions approach the 2D, diffusive case.

As the chamber diameter is increased, convective flows cause a drop in the maximum attainable supersaturation and

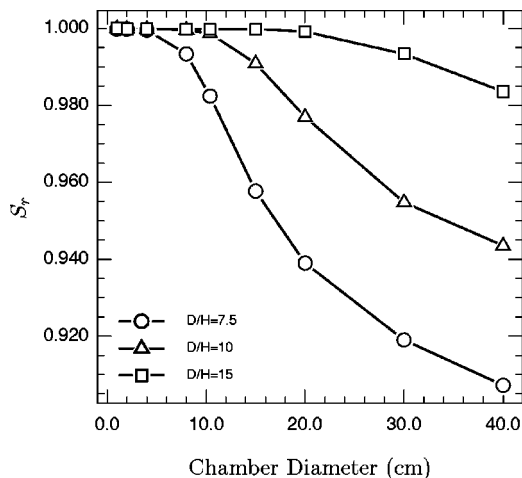


FIG. 5. Effect of chamber size on maximum supersaturation ratio. Results are shown for aspect ratios of $D/H=15$, $D/H=10$, and $D/H=7.5$.

the effect is more pronounced for the lower aspect ratio chambers. These results are computed for the critically heated case; if the chamber is overheated significantly, this heating may cause a further depression in the maximum supersaturation. Again, these results are for specific cases, but they clearly indicate that smaller chamber volumes and higher chamber aspect ratios are preferable.

E. General recommendations

The previous cases provided a glimpse of the effect of some parameters on the operation of the TDCC. In the case of a heated wall, as the convection increases it reduces the maximum attainable supersaturation within the nucleation chamber.

It is possible to provide some general recommendations on minimizing convection within the chamber by looking at a simplification of the governing equations used in this work. An important simplification often used in problems involving free convection is the Boussinesq approximation. This approximation is valid for systems in which density differences are small. For a full description of the approximation and the conditions under which it is valid see Ref. 19. Under this approximation all physical properties, including density, are taken to be constant except for the body force term, ρg , in the momentum equations. In this case, the density is rewritten as a linear function of temperature (and/or concentration). The TDCC is typically operated with heated walls and the density differences driving any buoyant flows are caused by the temperature gradient at the wall. Therefore, for the purposes of illustration, consider only density changes due to temperature changes—a similar argument also holds for concentration-induced density changes. Casting the density into a linear function of the temperature gives

$$\rho = \rho_0 + \left. \frac{\partial \rho}{\partial T} \right|_{T_0, w_{a_0}} (T - T_0) + \dots, \quad (26)$$

where the subscript 0, represents a reference condition. This equation can be rewritten as

$$\rho = \rho_0 + \rho_0 \beta (T - T_0) + \dots, \quad (27)$$

where β is the thermal expansion coefficient and is defined as

$$\beta = - \left. \frac{1}{\rho_0} \frac{\partial \rho}{\partial T} \right|_{T_0, w_{a_0}}. \quad (28)$$

Under the Boussinesq approximation, the governing equations can be written in non-dimensional form and for a given set of boundary conditions and aspect ratio, are governed by the Rayleigh number

$$\text{Ra} = \frac{g \beta \Delta T D^3 \rho^2 C_p}{\mu k}, \quad (29)$$

which represents the ratio of the destabilizing buoyancy forces to the retarding, viscous forces. The Rayleigh number in Eq. (29) is written for buoyancy effects arising from thermal variations and involves a characteristic temperature difference, $\Delta T = (T_{\text{lower}} - T_{\text{upper}})$. For an ideal gas, the term, β , is simply equal to $1/T$. If the other density terms are expanded using the ideal gas equation for the vapor-gas mixture the Rayleigh number becomes

$$\text{Ra} = \frac{g \Delta T D^3 P^2 M_w^2 C_p}{\mu k R^2 T^3}. \quad (30)$$

As Ra increases, buoyancy-induced convection increases. Examination of this term highlights some recommendations noted by other researchers on the stable operation of thermal diffusion cloud chambers. Namely, convection will be minimized for higher thermal conductivity, lower molecular weight gases, and higher absolute temperatures. One point not noticed to date is that, for a given aspect ratio, lower overall chamber volumes (as given by the characteristic length, D) will result in lower values of convective disturbances.

IV. CONCLUSIONS

We have developed a model of the energy and mass transport operations within a thermal diffusion cloud chamber which includes buoyancy-induced convective transport. We have used this model to study the wet and dry operation of an example case of 1-propanol in helium. For dry chamber operation, previous models were unable to show that wall heating of the thermal diffusion cloud chamber resulted in departures from the 1D results, even for considerable overheating. In contrast, by including convective effects we are able to show that there can be differences in the calculated maximum supersaturation even for critical wall heating. In this representative case, a subtle downward flow along the centerline results in a decreasing maximum supersaturation with increasing wall heat.

Unfortunately, as models tend to become more realistic, they often become less general and the model developed in this work has only been applied to one specific case. It is important to stress that even though heating of the walls resulted in a decreased maximum supersaturation, this is not a general statement that all wall heating will result in errors in supersaturation measurements. Whether or not significant

buoyant convection will develop depends on a variety of factors including the type of carrier gas used, the chamber dimensions, the condensible species being investigated, etc.

Although this work does not provide general quantitative criteria for the stable operation of the TDCC, it does provide general guidelines for the minimization of buoyant convection. Some of these have been highlighted before; for example using low molecular weight background gases and operating at higher absolute temperatures. One new feature found in this work is that convection is minimized for small chamber volumes due to the viscous damping effects of the chamber's boundaries. Therefore, results for two different size cloud chambers under identical operating conditions and aspect ratio can be different due to stronger convective flows in the larger chamber.

¹J. L. Katz and B. J. Ostermier, *J. Chem. Phys.* **47**, 478 (1967).

²J. L. Katz, J. A. Fisk, and V. M. Chakarov, *J. Chem. Phys.* **101**, 2309 (1994).

³D. Kane, G. M. Daly, and M. S. El-Shall, *J. Phys. Chem.* **99**, 7867 (1995).

⁴G. S. Cha, H. Uchtmann, J. A. Fisk, and J. L. Katz, *J. Chem. Phys.* **101**, 459 (1994).

⁵C. Hung, M. J. Krasnopoler, and J. L. Katz, *J. Chem. Phys.* **90**, 1856 (1989).

⁶B. E. Wyslouzil, G. Wilemski, M. G. Beals, and M. B. Frish, *Phys. Fluids* **6**, 2845 (1994).

⁷R. H. Heist, M. Janjua, and J. Ahmed, *J. Phys. Chem.* **98**, 4443 (1994).

⁸R. H. Heist, J. Ahmed, and M. Janjua, *J. Phys. Chem.* **99**, 375 (1995).

⁹R. H. Heist, *J. Phys. Chem.* **99**, 16792 (1995).

¹⁰A. Bertelsmann, R. Stuczynski, and R. H. Heist, *J. Phys. Chem.* **100**, 9762 (1996).

¹¹A. Bertelsmann and R. H. Heist, *J. Chem. Phys.* **106**, 610 (1997).

¹²A. Bertelsmann and R. H. Heist, *J. Chem. Phys.* **106**, 624 (1997).

¹³A. L. Itkin, *Chem. Phys.* **238**, 273 (1998).

¹⁴J. A. Fisk and J. L. Katz, *J. Chem. Phys.* **104**, 8649 (1996).

¹⁵*Fluid Flow Data Book* (Genium, Schenectady, NY, 1970).

¹⁶R. B. Bird, W. E. Stewart, and E. N. Lightfoot, *Transport Phenomena* (Wiley, New York, 1960).

¹⁷S. Patankar, *Numerical Heat Transfer and Fluid Flow* (Hemisphere, Washington, DC, 1980).

¹⁸J. A. Fisk, V. M. Chakarov, and J. L. Katz, *J. Chem. Phys.* **104**, 8657 (1996).

¹⁹P. Kundu, *Fluid Mechanics* (Academic, San Diego, CA, 1990).